TeoNAM: A Nested Association Mapping Population for Domestication and Agronomic Trait Analysis in Maize

Qiuyue Chen,*,† Chin Jian Yang,* Alessandra M. York,* Wei Xue,*,[1] Lora L. Daskalska,* Craig A. DeValk,* Kyle W. Krueger,* Samuel B. Lawton,* Bailey G. Spiegelberg,* Jack M. Schnell,* Michael A. Neumeyer,* Joseph S. Perry,* Aria C. Peterson,* Brandon Kim,* Laura Bergstrom,* Liyan Yang,*,‡ Isaac C. Barber,* Feng Tian,† and John F. Doebley*,[2]

*Laboratory of Genetics, University of Wisconsin–Madison, Wisconsin 53706, †National Maize Improvement Center, Key Laboratory of Biology and Genetic Improvement of Maize (MOA), Beijing Key Laboratory of Crop Genetic Improvement, Joint International Research Laboratory of Crop Molecular Breeding, China Agricultural University, Beijing 100193, China, and ‡School of Life Science, Shanxi Normal University, Linfen, Shanxi 041004, China

ORCID IDs: 0000-0002-3304-8321 (Q.C.); 0000-0003-0232-1521 (W.X.); 0000-0002-3421-9866 (L.Y.); 0000-0003-3552-4536 (F.T.); 0000-0003-1696-7112 (J.F.D.)

ABSTRACT Recombinant inbred lines (RILs) are an important resource for mapping genes controlling complex traits in many species. While RIL populations have been developed for maize, a maize RIL population with multiple teosinte inbred lines as parents has been lacking. Here, we report a teosinte nested association mapping (TeoNAM) population, derived from crossing five teosinte inbreds to the maize inbred line W22. The resulting 1257 BC_1S_4 RILs were genotyped with 51,544 SNPs, providing a high-density genetic map with a length of 1540 cM. On average, each RIL is 15% homozygous teosinte and 8% heterozygous. We performed joint linkage mapping (JLM) and a genome-wide association study (GWAS) for 22 domestication and agronomic traits. A total of 255 QTL from JLM were identified, with many of these mapping near known genes or novel candidate genes. TeoNAM is a useful resource for QTL mapping for the discovery of novel allelic variation from teosinte. TeoNAM provides the first report that *PROSTRATE GROWTH1*, a rice domestication gene, is also a QTL associated with tillering in teosinte and maize. We detected multiple QTL for flowering time and other traits for which the teosinte allele contributes to a more maize-like phenotype. Such QTL could be valuable in maize improvement.

KEYWORDS RIL; TeoNAM; JLM; GWAS; maize; domestication; multiparental populations; MPP

RECOMBINANT inbred line (RIL) populations are powerful tools for investigating the genetic architecture of traits and identifying the causal genes that underlie trait variation. RIL populations have been widely used in many organisms. In mammals, the well-known Collaborative Cross, consisting of a large panel of mouse multiparental RILs, has been specifically designed for the analysis of complex traits (Churchill *et al.* 2004). Similarly, the *Drosophila* Synthetic Population Resource (DSPR), which consists of two sets of RILs, has been designed to combine the high mapping resolution offered by multiple generations of recombination with the high statistical power afforded by a linkage-based design (King *et al.* 2012). In plants, the maize nested association mapping (NAM) population, which crossed 25 founders to a common parent in maize (Yu *et al.* 2008), has been successfully applied to a large number of traits (Buckler *et al.* 2009; Kump *et al.* 2011; Tian *et al.* 2011). The NAM design has also been utilized in other crops such as barley (Maurer *et al.* 2015; Nice *et al.* 2016), rice (Fragoso *et al.* 2017), sorghum (Bouchet *et al.* 2017), wheat (Jordan *et al.* 2018), and soybean (Xavier *et al.* 2018). In *Arabidopsis*, another design,

doi: https://doi.org/10.1534/genetics.119.302594
Manuscript received August 5, 2019; accepted for publication August 30, 2019; published Early Online September 3, 2019.
Available freely online through the author-supported open access option.
Supplemental material available at Figshare: https://doi.org/10.25386/genetics.9250682.
[1]Present address: College of Agronomy, Shenyang Agricultural University, Shenyang, Liaoning 110866, China.
[2]Corresponding author: Laboratory of Genetics, University of Wisconsin–Madison, 425 Henry Mall, Madison, WI 53706. E-mail: jdoebley@wisc.edu

called the Multiparent Advanced Generation Intercross (MAGIC) population, provides high precision for the detection of QTL (Kover *et al.* 2009; Huang *et al.* 2011). This design has also been used in wheat (Huang *et al.* 2012; Mackay *et al.* 2014), rice (Bandillo *et al.* 2013), and maize (Dell'Acqua *et al.* 2015).

For the study of maize domestication, many new discoveries were made using a biparental maize–teosinte BC_2S_3 RIL population. Shannon (2012) performed QTL mapping for 16 traits and examined the genetic architecture of domestication at the whole-genome level. This RIL population has also been widely used to fine-map QTL, and identify causal or candidate genes for many traits, including seed shattering (Lin *et al.* 2012), leaf number (Li *et al.* 2016), kernel row number (KRN) (Calderón *et al.* 2016), shoot apical meristem morphology (Leiboff *et al.* 2016), vascular bundle number (Huang *et al.* 2016), tassel-related traits (G. Xu *et al.* 2017), nodal root number (Zhang *et al.* 2018), and leaf morphological traits (Fu *et al.* 2019). Using this population, several QTL have been fine-mapped to single genes including *grassy tillers1* (*gt1*) for controlling prolificacy (PROL) (Wills *et al.* 2013), *prolamin box-binding factor1* (*pbf1*) for kernel weight (Lang *et al.* 2014), *glossy15* (*gl15*) for vegetative phase changes (D. Xu *et al.* 2017), *UPA1* (*Upright Plant Architecture1*) and *UPA2* for leaf angle (Tian *et al.* 2019), as well as several genes regulating flowering time: *ZmCCT10* (Hung *et al.* 2012), *Zea Agamous-like1* (*zagl1*) (Wills *et al.* 2017), *ZmCCT9* (Huang *et al.* 2018), *Zea mays CENTRORADIALIS8* (*ZCN8)* (Guo *et al.* 2018), and *MADS-box transcription factor69* (*ZmMADS69*) (Liang *et al.* 2019). In addition to phenotypic traits, the maize–teosinte BC_2S_3 RIL population was used for comprehensive genome-wide expression QTL (eQTL) analysis to study the changes in gene expression during maize domestication (Wang *et al.* 2018), and metabolite QTL analysis to study metabolic divergence between maize and teosinte (Xu *et al.* 2019).

Despite its utility, the maize–teosinte BC_2S_3 RIL population has three limitations. First, there is only a single teosinte parent, which cannot broadly represent the diversity of teosinte. Second, this population had two generations of backcrossing, which has produced a background in which some teosinte traits are suppressed and do not segregate among the RILs. Third, the teosinte parent was a wild outcrossed individual which, unlike an inbred line, could not be maintained as a permanent resource.

In this paper, we report the development of a teosinte NAM (TeoNAM) population of 1257 BC_1S_4 RILs using five teosinte inbred parents crossed with a common maize parent (W22) for mapping QTL for domestication and agronomic traits. We have genotyped the RILs with 51,544 genotype-by-sequencing (GBS) markers that provide a high-density genetic map. The TeoNAM population captures a large number of recombination events for localizing QTL to genomic locations and the single generation of backcross allows enhanced expression of teosinte traits as compared to the BC_2S_3 RIL population. We report data for 22 traits but focus our discussion on nine traits to illustrate the utility of TeoNAM, including the identification of candidate genes. TeoNAM will be a valuable resource for dissecting the genetic basis of domestication and agronomic traits.

Materials and Methods

Population development

The TeoNAM population was designed as a genetic resource for studying maize genetics and domestication. Five wild teosinte parents were chosen, with four teosinte inbred lines that capture some diversity of *Z. mays* ssp. *parviglumis* (TIL01, TIL03, TIL11, and TIL14) and one teosinte inbred line of *Z. mays* ssp. *mexicana* (TIL25). The common parent is a modern maize inbred line (W22) that has been widely used in maize genetics. The five teosinte parents were crossed to W22, and followed by one generation of backcrossing and four generations of selfing (Supplemental Material, Figure S1). We obtained 1257 BC_1S_4 RILs with 223, 270, 219, 235, and 310 lines for W22 × TIL01, W22 × TIL03, W22 × TIL11, W22 × TIL14, and W22 × TIL25, respectively.

Marker data

All DNA samples of 1257 lines were genotyped using GBS technology (Elshire *et al.* 2011). The genotypes were called from GBS raw sequencing reads using the TASSEL5-GBS Production Pipeline based on 955,690 SNPs in the ZeaGBSv2.7 Production TagsOnPhysicalMap file (Glaubitz *et al.* 2014). Then, the raw GBS markers were filtered in each RIL subpopulation using the following steps. We first removed sites with minor allele frequencies (MAFs) $< 5\%$ and thinned sites 64-bp apart using "Thin Sites by Position" in TASSEL5 (Bradbury *et al.* 2007), and then we ran FSFHap Imputation in TASSEL5 separately for each chromosome using the following parameters: backcross, Phet = 0.03125, Fillgaps = TRUE, and the default settings for other features. The imputed parental call files from the 10 chromosomes were then combined together and passed to R/qtl (Broman *et al.* 2003) to estimate the genetic map. The B73 reference genome v2 was used to determine marker order, and genetic distances between markers were calculated using the Haldane mapping function as part of the *est.map* command with an assumed genotyping error rate of 0.001, taking the BC_1S_4 pedigree of the RIL into consideration (Shannon 2012). Bad genetic markers were identified by visual inspection of the genetic map and removed, then we repeated all filtering steps. Finally, an average of 13,733 high-quality SNPs was obtained for each subpopulation (Table 1).

Field design and phenotyping

The TeoNAM population was planted using a randomized complete block design at the University of Wisconsin West Madison Agricultural Research Station in different years. The subpopulations W22 × TIL01, W22 × TIL03, and W22 × TIL11 were grown in summer 2015 and 2016, subpopulation W22 × TIL14 was grown in summer 2016 and 2017, and subpopulation W22 × TIL25 was grown in summer 2017 with two blocks. We

planted one subpopulation within each block and all lines were randomized within each block. Each row had 16 seeds planted 1-ft apart, and spacing between any two rows was 30 in.

Twenty-two traits were scored (Table 2): days to anthesis (DTA) (number of days between planting and when at least one-half of the plants in a plot were shedding pollen); days to silk (DTS) (number of days between planting and when at least one-half of the plants in a plot were showing silk); anthesis–silk interval (ASI) (number of days between anthesis and silk); tassel branch number (TBN) (number of tassel branches on the main stalk); culm diameter (CULM) (diameter of the narrowest plane of the main stalk right above the ground); plant height (PLHT) (distance from the ground to the topmost node on the main stalk); leaf length (LFLN) (length of a well-developed leaf, usually fourth to sixth from top); leaf width (LFWD) (width of a well-developed leaf, usually fourth to sixth from top); tiller number (TILN) (number of tillers surrounding main stalk); PROL (0 *vs.* 1 for absence/presence of secondary ears at the topmost branch-bearing node on the main stalk); ear branch number (EB) (number of branches on the primary lateral inflorescence); staminate spikelet (STAM) (0–3 scale for spikelet sex on the primary lateral inflorescence, where 0 indicates completely feminized and 3 indicates completely staminate); KRN (number of internode columns on the primary lateral inflorescence); ear length (EL) (length of the primary lateral inflorescence); ear diameter (ED) (diameter of the primary lateral inflorescence); kernel weight (KW) (average weight of 50 random kernels from five ears); shattering (SHN) (number of pieces into which an ear shatters when dropped to the floor from a height of ~1.8 m); barren ear base (BARE) (0–2 scale for lack of kernels at the base of the ear, where 0 indicates kernels present at the base and 2 indicates no developed kernels at the base of the ear); glume score (GLUM) (0–3 scale for glume size, where 0 indicates small and 3 indicates large); glume color (GLCO) (0–4 scale of glume color for white through brown); red pericarp (REPE) (0–2 scale for colorless to red pericarp); and yellow pericarp (YEPE) (0–2 scale for dull yellow to bright yellow pericarp). The average trait values from 2 years were used for QTL analysis.

Genetic map construction and marker imputation

A composite genetic map was constructed for the TeoNAM population. The markers from the five RIL subpopulations were combined together into 51,544 unique SNPs, and the missing genotypes were imputed according to the flanking markers. If the flanking markers had same genotypes, the missing genotype was imputed as the same with flanking markers, or otherwise left as missing. The imputed genotypes were then passed to R/qtl software to estimate the genetic map.

Since stepwise regression cannot use individuals with missing marker data, we performed a further step to impute missing data around breakpoint as previously described (Tian *et al.* 2011). First, we transformed genotypes to a numeric format, in which markers with a homozygous W22 parent were coded as 0, markers with a homozygous non-W22 parent were coded as 2, and markers with heterozygous genotypes were coded as 1. Markers within breakpoint were imputed according to the genetic distance of flanking two markers. Because stepwise regression is computationally intensive, we thinned SNPs within 0.1 cM. We finally obtained 4578 markers for subsequent joint linkage analysis.

Simple QTL mapping

QTL mapping was carried out using a modified version of R/qtl (Broman *et al.* 2003), which takes into account the BC_1S_4 pedigree of the RILs (Shannon 2012). For each trait, a total of 1000 permutation tests were used to determine the significance threshold levels for claiming QTL. After permutation, an approximate LOD score of 4.0 at $P < 0.05$ was obtained across all traits. With the LOD threshold, simple interval mapping was first fitted using Haley–Knott regression implemented in the *scanone* command of R/qtl. The multiple QTL model was then applied to search for additional QTL, and accurately refine QTL positions using *refineqtl* and *addqtl* in R/qtl. The entire process was repeated until significant QTL could no longer be added. The total phenotypic variation explained by all QTL was calculated from a full model that fitted all QTL terms in the model using the *fitqtl* function. The percentage of phenotypic variation explained by each QTL was estimated using a drop-one ANOVA analysis implemented with the *fitqtl* function. The C.I. for each QTL was defined using a 1.5-LOD support interval. To make results comparable among five subpopulations, the composite genetic map was used for QTL mapping.

Joint linkage mapping

To map QTL in the TeoNAM population, a joint linkage mapping (JLM) procedure was performed as previously described (Buckler *et al.* 2009; Tian *et al.* 2011). First, a total of 1000 permutations were performed to determine the significance cutoff for each trait. JLM was performed using the stepwise linear regression fixed model implemented by the PROC GLMSELECT procedure in SAS software. The family main effect was fitted first, and then marker effects nested within families were selected to enter or leave the model based on the permutated *P*-value using a marginal *F*-test. After the model was fitted with stepwise regression, each marker was dropped from the full model one at a time and a single best marker was refitted to improve the overall fit of the model. A threshold of $\alpha = 0.05$ was used to declare significant allele effects across families within each QTL identified by stepwise regression. The QTL support interval was calculated by adding each marker from the same chromosome of that QTL at a time to the full model. If the *P*-value of the marginal *F*-test of the QTL was not significant at the 0.01 level, the flanking marker should be in the support interval for the QTL, as the new flanking marker explained the QTL as well as the original marker.

Genome-wide association study

A genome-wide association study (GWAS) approach was also used to map QTL in the TeoNAM population. Since GBS produces relatively low-density markers, the 955,690 raw SNPs

Table 1 TeoNAM genetic map statistics

Population	No. RILs	No. Markers	Length (cM)	No. XOs	cM/Mb	W22 (%)	Heterozygous (%)	Teosinte (%)
W22 × TIL01	223	13,088	1457	6,291	0.71	75.8	7.7	16.0
W22 × TIL03	270	16,109	1596	8,505	0.78	75.5	8.1	16.2
W22 × TIL11	219	13,187	1398	5,745	0.68	76.3	7.6	15.6
W22 × TIL14	235	11,395	1348	6,462	0.65	75.7	9.4	14.6
W22 × TIL25	310	14,884	1506	8,877	0.73	77.6	8.0	14.2
Composite	1257	51,544	1540	35,880	0.75	76.6	8.1	15.0

No., number; RIL, recombinant inbred line; XO, crossover.

from the GBS pipeline were filtered using less-conservative criteria: MAF > 0.01, missing rate < 0.75, and heterozygosity rate < 0.1. After this filtering, 181,404 GBS SNPs were used to run FSFHap Imputation in TASSEL5 separately for each chromosome and subpopulation using the following parameters: backcross, Phet = 0.03125, Fillgaps = TRUE, and the default settings for other features. Imputed genotypes were then combined together, and SNPs with missing rate > 0.2 and MAF $<$ 0.05 across 1257 RILs were removed, and a total of 118,838 SNPs were kept and used for GWAS. GWAS was performed using a linear mixed model accounting for population structure (Q) and kinship matrix (K), where Q was computed as the first five principle components and K was calculated using a centered Identity-By-State (IBS) method as implemented in TASSEL (Bradbury *et al.* 2007). *P*-values $< P = 0.00001$ (LOD = 5) were considered to be the significance threshold, following a previous study (Kremling *et al.* 2018).

QTL candidate analysis

To report the QTL position following the latest genomic version, we used the CrossMap (Zhao *et al.* 2014) software to uplift the GBS SNP positions from maize B73 reference AGPv2 coordinates to AGPv4 coordinates. QTL candidates were analyzed by checking the gene annotations of genes within QTL support intervals.

Data availability

Seeds for all 1257 RILs in TeoNAM are available at the Maize Genetics Cooperative Stock Center. The SNP genotypes for TeoNAM are available at the Cyverse Discovery Environment under the directory: http://datacommons.cyverse.org/browse/iplant/home/shared/panzea/genotypes/GBS/TeosinteNAM. The genotypic data were uploaded with AGPv2 position in the marker name. The raw phenotypic data for TeoNAM are available at Figshare database: https://doi.org/10.6084/m9.figshare.9820178. The seed information, SNP genotypes, and phenotypic data for the BC_2S_3 maize–teosinte RIL population can be found in Shannon *et al.* (2019). Supplemental material available at Figshare: https://doi.org/10.25386/genetics.9250682.

Results

Characterization of a TeoNAM population

We developed a TeoNAM population, which was constructed by crossing five teosinte inbred lines to a maize inbred line (W22), followed by one generation of backcross to the common recurrent maize parent and four generations of selfing (Figure S1). The teosinte parents include four *Z. mays* ssp. *parviglumis* lines and one *Z. mays* ssp. *mexicana* line. As such, TeoNAM encompasses five biparental families, each with 219–310 BC_1S_4-derived RILs for a total of 1257 RILs. The number of segregating SNP markers ranges from 11,395 to 16,109 per family, with over 51,000 total SNP markers (Table 1).

The expected segregation for a BC_1S_4 population is 73.44% homozygous recurrent, 3.13% heterozygous, and 23.44% homozygous donor parent. Overall, the percentage of genotypes observed were 76.6% W22 homozygous, 15% teosinte homozygous, and 8.1% heterozygous across all SNP sites in the TeoNAM population (Table 1). The percentage of teosinte varied among subpopulations from 14.2 to 16.2% (Table 1), and also varied across the genome in all subpopulations (Figure S2). The observed higher than expected heterozygosity may be due to unconscious selection for more heterozygous plants that had hybrid vigor. The chromosomal region of highest heterozygosity is on the short arm of chromosome 4 near *teosinte glume architecture1* (*tga1*) (Wang *et al.* 2005). Selection against homozygotes for the teosinte allele of *tga1*, which have poor ear and kernel quality, may be the cause. For a BC_1S_4, the expected frequency of the maize allele is 75%. All subpopulations deviate from this with an excess of maize alleles (Table 1) and the amount of excess varies across the genome (Figure S3).

We constructed genetic linkage maps for each family and a composite linkage map based on all RILs across all families, and identified and annotated 51,544 high-confidence SNPs that were used to impute the SNP alleles in the RILs. The composite genetic map based on these markers is 1540 cM in length including 35,880 crossovers. We examined the relationship between genetic distance in centimorgans and physical distance in megabases based on the composite genetic map. The mean value is 0.75 cM/Mb. However, there is wide deviation from the mean across the genome (0–5.52 cM/Mb). As expected, there is suppressed recombination near the centromeres (Figure S2) and frequent recombination near the telomeres, where gene density is high as well (Figure S2).

We scored 22 traits for the TeoNAM lines of which 15 traits are domestication related, including vegetative gigantism (CULM, LFLN, and LFWD), prolificacy (PROL), tillering (TILN), ear SHN, conversion of the inflorescence from staminate to pistillate (STAM), multiple ear-related traits (EB, ED, EL, KRN, and KW), glume traits (GLCO and GLUM), and REPE

Table 2 List of 22 domestication and agronomic traits scored

Trait	Abbreviation	Units	Category
Anthesis–silk interval	ASI	count	Agronomic
Barren ear base	BARE	score	Agronomic
Days to anthesis	DTA	count	Agronomic
Days to silk	DTS	count	Agronomic
Plant height	PLHT	cm	Agronomic
Tassel branch number	TBN	count	Agronomic
Yellow pericarp	YEPE	score	Agronomic
Culm diameter	CULM	mm	Domestication
Ear branch number	EB	count	Domestication
Ear diameter	ED	mm	Domestication
Ear length	EL	cm	Domestication
Glume color	GLCO	score	Domestication
Glume score	GLUM	score	Domestication
Kernel row number	KRN	count	Domestication
Kernel weight	KW	g	Domestication
Leaf length	LFLN	cm	Domestication
Leaf width	LFWD	cm	Domestication
Prolificacy	PROL	binary	Domestication
Red pericarp	REPE	score	Domestication
Shattering	SHN	count	Domestication
Staminate spikelet	STAM	score	Domestication
Tiller number	TILN	count	Domestication

(Table 2). Additionally, several agronomic traits were scored including flowering (ASI, DTA, and DTS), plant architecture (PLHT and TBN), BARE, and YEPE. Most traits (ASI, CULM, DTA, DTS, ED, EL, KRN, KW, LFLN, LFWD, PHLT, and TBN) follow approximately normal distributions, suggesting oligo- or polygenic genetic control of these traits, but other traits (BARE, EB, GLCO, GLUM, PROL, REPE, SHN, STAM, TILN, and YEPE) exhibited a skewed or nonnormal distribution. Some of these traits are meristic or discrete traits (*e.g.*, PROL or TILN). A few traits, like STAM, show a two-part distribution with a spike at 0 plus a continuous range of values from 0 to 2, which suggests that they may be polygenic threshold traits (Figure S4). There are also substantial differences in trait means among the five subpopulations, indicating underlying differences in genetic architecture among the five teosinte inbreds (Figure S5).

Validation of the power of TeoNAM

QTL mapping: We used both JLM and the GWAS method as two complementary approaches for QTL detection. We also used basic interval QTL mapping for the five individual subpopulations to provide a guide for future work to fine-map the genes underlying the QTL. We detected 255 QTL for 22 traits by JLM, which combines information across all families (Figure 1 and Table S1). We detected a total of 150 QTL by GWAS, among which 57 QTL overlapped with QTL by JLM (Table S2). Separate QTL mapping for each subpopulation detected 464 QTL in total, among which 293 QTL overlapped with QTL by JLM (Figures S6–S27 and Table S3). Below, we focus on QTL detected by JLM for our characterization of the genetic architecture and the distribution of QTL allelic effects.

Among 22 traits, the numbers of QTL range from 2 to 24; the trait with the most QTL is KRN. Genetic architecture varies considerably among traits (Figure 2 and Figure S28). Several traits—including BARE, GLCO, GLUM, PROL, REPE, and STAM—had relatively simple genetic architectures, with a single QTL of very large effect plus a few (3–10) QTL of small effect. The largest QTL for each of these traits has between 2.1 and 11.7 times the size of the effect of the second largest QTL. A second class of traits has a genetic architecture that is either more polygenic (ED, KRN, KW, LFLN, TBN, and TILN) or has only a few QTL of small effect (ASI, CULM, EB, LFWD, PLHT, and SHN). For these traits, there was no single large-effect QTL that accounts for the majority of the explainable variation. The largest effect QTL for each of these traits has between 1 and 1.8 times the size of the effect of the second largest QTL. A final class of traits has a genetic architecture with both a single QTL of moderately large effect plus multiple (11–19) QTL of small effect. These traits include DTA, DTS, EL, and YEPE. The largest effect QTL for each of these traits is between 2.1 and 3.7 times the size of the effect of the second largest QTL.

QTL for agronomic traits: DTA is a classical quantitative trait for maize, and in TeoNAM, it is controlled by a large-effect QTL plus many small-effect QTL from JLM results. We detected 19 QTL that explained 68% of the total variance for DTA (Figure 3). Among them, several recently cloned flowering time genes were detected. For example, *zagl1* was included within QTL *DTA1.1*, which affects flowering time as well as multiple traits related to ear size, with the maize allele conferring larger ears with more kernels (Wills *et al.* 2017). *ZmMADS69* was included within QTL *DTA3.1*, which functions as a flowering activator through the *ZmRap2.7-ZCN8* regulatory module, and contributes to both long-day and short-day adaptation (Liang *et al.* 2019). *ZCN8* was included within QTL *DTA8.1*, which is the maize florigen gene and has a central role in mediating flowering (Meng *et al.* 2011; Guo *et al.* 2018). *ZmCCT9* was included within QTL *DTA9.1*, in which a distant Harbinger-like transposon acts as a *cis*-regulatory element to repress its expression to promote flowering under the long days of higher latitudes (Huang *et al.* 2018). *ZmCCT10* was included within QTL *DTA10.1*, which is a known gene involved in the photoperiod response in maize (Hung *et al.* 2012; Yang *et al.* 2013).

In addition to these genes, we also identified several other candidate genes for DTA that have not previously been characterized as genes underlying a QTL. *Z. mays CENTRORADIALIS12* (*ZCN12*) was included within QTL *DTA3.2*, which is a potential floral activator (Meng *et al.* 2011). *Z. mays MADS19* (*Zmm19*) was included within QTL *DTA4.1* and *Z. mays MADS31* (*Zmm31*) was included within *DTA5.1*. *silky1* (*si1*) was included within QTL *DTA6.1*, which is also a MADS-box gene required for lodicule and stamen identity (Ambrose *et al.* 2000). *Zea AGAMOUS1* (*ZAG1*) was included within QTL *DTA6.2*, which is known to affect maize flower development (Schmidt *et al.* 1993). It is well known that

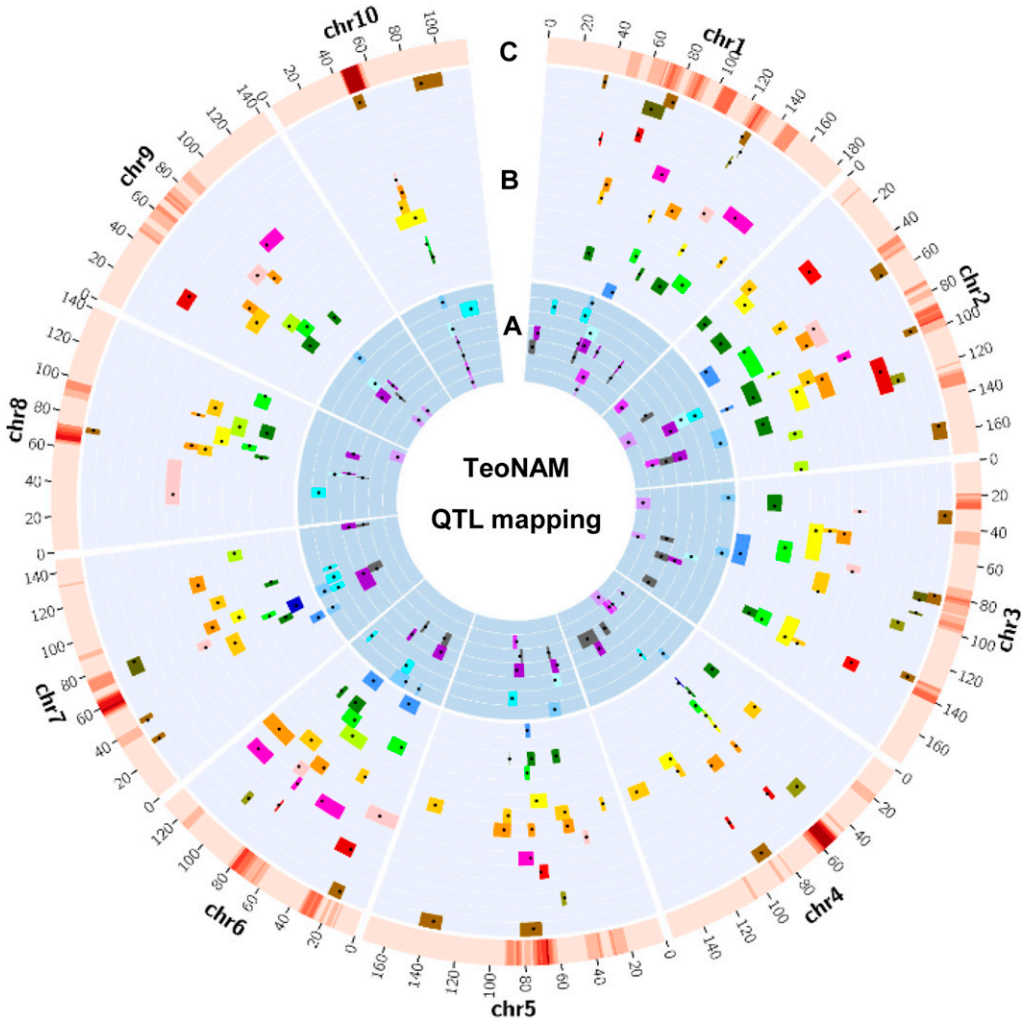

Figure 1 Genomic distribution of QTL for all 22 traits in TeoNAM. The 22 agronomic (A) and domestication (B) traits are plotted in layers with different background colors, following the order of ASI, BARE, DTA, DTS, PLHT, TBN, YEPE, CULM, EB, ED, EL, GLCO, GLUM, KRN, KW, LFLN, LFWD, PROL, REPE, SHN, STAM, and TILN outward. Black dots indicate QTL peaks detected by JLM and colored bars indicate the support interval of QTL for different traits. The heat map in the outmost layer (C) shows the number of QTL peaks using a sliding window of 10- and 1-cM steps, where low-to-high densities of QTL (0–13) are shown in light-to-dark red, respectively. ASI, anthesis–silk interval; BARE, barren ear base; DTA, days to anthesis; DTS, days to silk; CULM, culm diameter; EB, ear branch number; ED, ear diameter; EL, ear length; GLCO, glume color; GLUM, glume score; KRN, kernel row number; KW, kernel weight; LFLN, leaf length; LFWD, leaf width; PLHT, plant height; PROL, prolificacy; REPE, red pericarp; SHN, shattering; STAM, staminate spikelet; TBN, tassel branch number; TILN, tiller number; YEPE, yellow pericarp. chr, chromosome; JLM, joint linkage mapping; TeoNAM, teosinte nested association mapping.

MADS-box genes encode transcription factors that are key regulators of plant inflorescence and flower development (Theissen *et al.* 2000). Other than MADS genes, *delayed flowering1* (*dlf1*), a floral activator gene downstream of *ZCN8* (Meng *et al.* 2011), was included within QTL *DTA7.2*.

As expected, the teosinte alleles delayed flowering for the above QTL that mapped to candidate genes (Figure 3). We plotted the phenotypic difference in DTA between teosinte and maize across the whole genome, and the teosinte genotype was associated with late flowering over most of the genome, even where no QTL were detected, suggesting that there are many additional minor-effect QTL that were not detected due to insufficient statistical power (Figure S29). Interestingly, chromosomes 5 and 7 are exceptions to this pattern, with the teosinte genotype being associated with early flowering at most sites (Figure S29). Results for DTS were similar to those for DTA, as expected (Figure S30).

TBN is the only tassel trait that we scored. We detected 12 QTL of small effect that explained 52% of the total variance for TBN (Figure S31). Among them, several classical genes were identified. *fasciated ear4* (*fea4*) was included within QTL *TBN6.1*, which is a bZIP transcription factor with fasciated ears and tassels, as well as greatly enlarged vegetative and inflorescence meristems (Pautler *et al.* 2015). *tasselsheath1* (*tsh1*) was included within QTL *TBN6.2*, which is a GATA class transcription factor that promotes bract growth and reduces branching (Whipple *et al.* 2010). *ramosa1* (*ra1*) was included within QTL *TBN7.1*, which is a C2H2 zinc finger transcription factor that has tassels with an increased number of long branches as well as branched ears (Vollbrecht *et al.* 2005). *tasselsheath4* (*tsh4*) was included within QTL *TBN7.2*, which is a SQUAMOSA promoter-binding protein (SBP)-box transcription factor that functions to repress lateral organ growth and also affects phyllotaxy, axillary meristem initiation, and meristem determinacy within the floral phase (Chuck *et al.* 2010). *Barren inflorescence1* (*Bif1*) was included within QTL *TBN8.1*, which shows decreased production of branches and spikelet pairs (Barazesh and McSteen 2008). *Zea floricaula leafy1* (*zfl1*) was included within QTL *TBN10.1*, which together with its homolog *zfl2* leads to a disruption of floral organ identity and patterning, as well as to defects in inflorescence architecture and in the vegetative-to-reproductive phase transition (Bomblies *et al.* 2003).

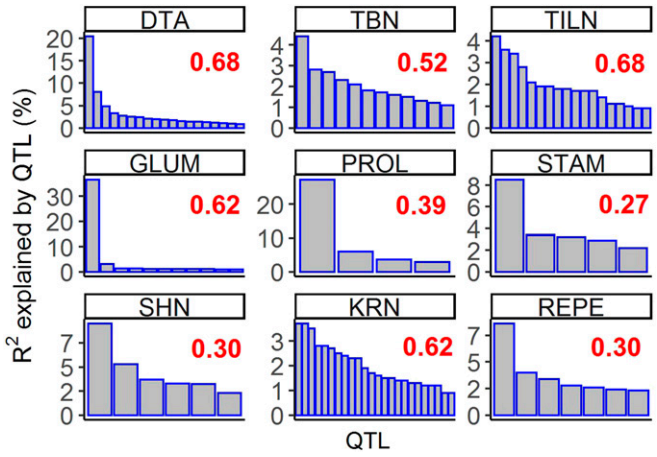

Figure 2 Distinct genetic architectures for different traits. The nine traits that we focused on in the main text are shown. The *x*-axes indicate QTL and the *y*-axes indicate the phenotypic variation explained by each QTL (R^2). Red numbers indicate variance explained by the QTL model for each trait. The R^2 distribution for 13 additional traits can be found in Figure S28. DTA, days to anthesis; GLUM, glume score; KRN, kernel row number; PROL, prolificacy; REPE, red pericarp; SHN, shattering; STAM, staminate spikelet; TBN, tassel branch number; TILN, tiller number.

QTL for domestication traits: TILN is a classical domestication trait that measures the difference in plant architecture between maize and its wild relative teosinte, *i.e.*, the low apical dominance of a highly branched teosinte plant as compared to the less-branched maize plant. We detected 18 small-effect QTL that explained 68% of the total variance for TILN (Figure S32). Among them, *teosinte branched1* (*tb1*) was included within QTL *TILN1.3*, which is a TCP family of transcriptional regulators contributing to the increase in apical dominance during maize domestication (Doebley *et al.* 1997). Additionally, *Zea AGAMOUS2* (*ZAG2*) was included within QTL *TILN3.2*, which is a MADS-box gene recently found to be downstream of *tb1* (Studer *et al.* 2017). *Zmm20* and *Zmm26* were included within QTL *TILN1.1* and *TILN5.2*, respectively, which are two other MADS-box genes that were possible targets of selection during domestication (Zhao *et al.* 2011). *PROSTRATE GROWTH1* (*PROG1*) was included within QTL *TILN7.1*, which is a C2H2 zinc finger protein controlling a key change during rice domestication from prostrate to erect growth, and also affecting plant architecture and yield-related traits (Jin *et al.* 2008; Tan *et al.* 2008). There are 13 genes in the support interval and the QTL peak is closest to *PROG1*, being ~14 kb 5′ of the start site (Figure S32). This is the first evidence that *PROG1* may have had a role in maize domestication.

GLUM is a classical maize domestication trait that measures the dramatic change from the fruitcase-enveloped kernels of the teosinte ear to the naked grains of maize ear. Previously, this trait was shown to be largely controlled by a single gene that is known as *teosinte glume architecture1* (*tga1*) (Wang *et al.* 2005, 2015). Interestingly, *tga1* is a direct target of *tb1*. We detected 11 QTL that explained 62% of the total variance for GLUM. These QTL include *tga1* itself within a large-effect QTL *GLUM4.1* plus several small-effect QTL (Figure S33). Among the small-effect QTL, two MADS genes (*Zmm27* and *Zmm7*) were included within *GLUM2.2* and *GLUM7.1*, respectively. In this regard, Studer *et al.* (2017) recently defined a maize domestication gene network in which *tga1* regulates multiple MADS-box transcription factors.

PROL is also an important domestication trait that measures the difference between the many-eared plants of teosinte and the few-eared (one or two) plants of maize. Previously, a large-effect QTL was fine-mapped to a region 2.7 kb upstream of *gt1* (Wills *et al.* 2013). Interestingly, *gt1* is a known target of *tb1* (Whipple *et al.* 2011). We detected four QTL that explained 39% of the total variance for PROL, which included a single large-effect QTL plus three small-effect QTL (Figure S34). Concordantly, *gt1* was included within QTL *PROL1.1*. The QTL *PROL3.1* support interval included *sparse inflorescence1* (*spi1*), which affects the initiation of axillary meristems and lateral organs during vegetative and inflorescence development in maize (Gallavotti *et al.* 2008).

STAM measures the proportion of the terminal lateral inflorescence on the uppermost lateral branch that is staminate. Relative to domestication, this trait represents the sexual conversion of the terminal lateral inflorescence from tassel (staminate) in teosinte to ear (pistillate) in maize. Currently, *tb1* and *tassels replace upper ears1* (*tru1*) are the only two genes that have been shown to regulate this sexual difference. We detected five QTL that explained 27% of the total variance for STAM (Figure 4). QTL *STAM1.2* mapped upstream of *tb1*, which is an important domestication gene known for various traits (Doebley *et al.* 1995). *tru1* was included within QTL *STAM3.1*, which is a direct target of *tb1* (Dong *et al.* 2017). *tassel seed2* (*ts2*) was included within QTL *STAM1.1*, which is a recessive mutant that produces pistillate spikelets in the terminal inflorescence (tassel) (Irish and Nelson 1993). *Z. mays MADS16* (*Zmm16*) was included within QTL *STAM3.2*. *tassel sheath4* (*tsh4*) was included within QTL *STAM7.1*, which is an SBP-box transcription factor that regulates the differentiation of lateral primordia (Chuck *et al.* 2010). In addition to these QTL, two other STAM QTL were detected by GWAS. Notably, a QTL on chromosome 1 (AGPv4 chromosome 1:234.4–249.9 Mb) is located upstream of *tb1* and colocalized with *STAM1.1* from a recent study (Yang 2018). The known gene *anther ear1* (*an1*) is a strong candidate gene for this QTL since loss of *an1* function results in the development of staminate flowers in the ears (Bensen *et al.* 1995). The *tb1* QTL region was also detected by GWAS with a strong signal (AGPv4 chromosome 1:264.1–283.1 Mb), which includes *tb1*.

SHN measures ear shattering, the loss of which is a key step during crop domestication (Doebley *et al.* 2006). Teosinte ears have abscission layers between the fruitcases (modified internodes) that allow the ear to shatter into single-seed units (fruitcase) at maturity. The maize ear lacks abscission layers and remains intact at maturity. Currently, only two maize orthologs (*ZmSh1-1* and *ZmSh1-5.1+ZmSh1-5.2*) of sorghum and rice *Shattering1* (*Sh1*) have been verified for seed

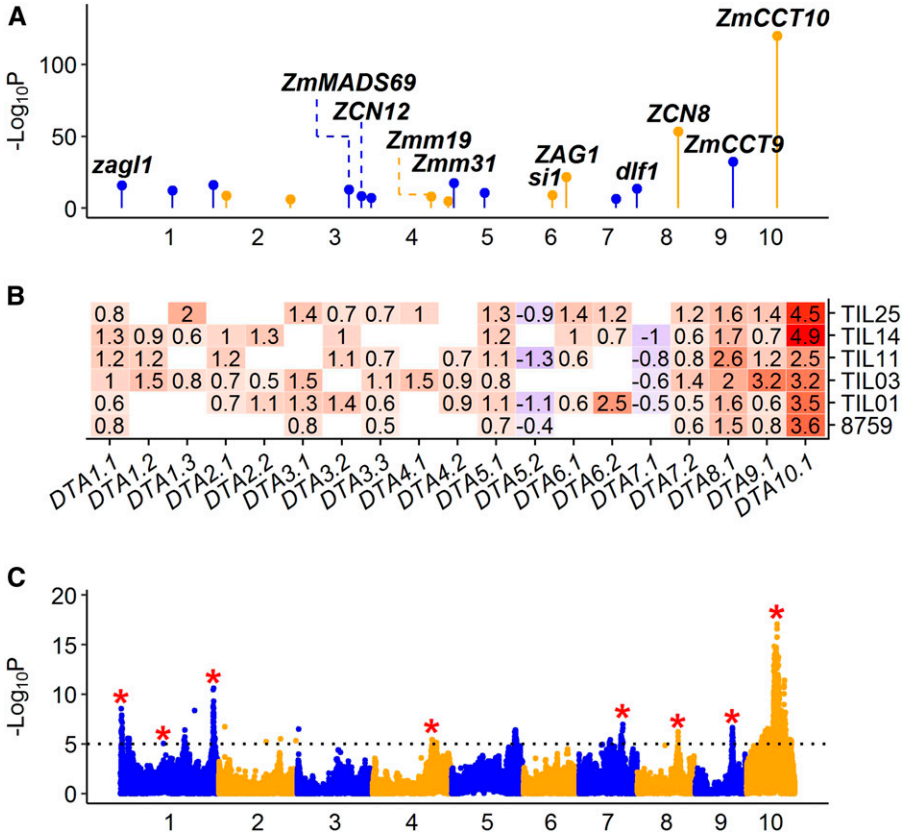

Figure 3 QTL characterization for agronomic trait DTA. (A) Genomic distribution of 19 QTL for DTA detected by JLM. The known candidate genes are shown above the corresponding QTL in bold italic. (B) Heat map shows additive allele effects of teosinte relative to maize in number of days for 19 QTL detected by JLM. The allele effect of teosinte parent 8759 was estimated from the 866 maize–teosinte BC_2S_3 RILs (Shannon 2012). Insignificant effects are shown as blank. Red and blue colors indicate that the teosinte alleles delay or promote flowering time, respectively. (C) Manhattan plot shows QTL detected by GWAS. The significance threshold at LOD = 5 is indicated by black dotted line. The red stars indicate GWAS signals overlapping with QTL by JLM. In (A) and (C), odd and even numbered chromosomes are shown in blue and orange colors, respectively. DTA, days to anthesis; GWAS, genome-wide association study; JLM, joint linkage mapping; RIL, recombinant inbred line.

SHN (Lin *et al.* 2012). We detected six QTL that explained 30% of the total variance for SHN (Figure S35). *Sh1-1* and *Sh1-5.1/5.2* were included within QTL *SHN1.1* and *SHN5.1*, respectively, confirming prior identification of these maize paralogs of the sorghum SHN gene as strong candidates for our QTL.

KRN is a domestication trait measuring the dramatic change from the two-ranked teosinte ear to a multiple-ranked (four or more) maize ear. We detected 24 small-effect QTL that explained 62% of the total variance for KRN (Figure S36). Among them, *indeterminate spikelet1* (*ids1*) was included within QTL *KRN1.3*, which is an APETALA2-like transcription factor that specifies determinate fates by suppressing indeterminate growth within the spikelet meristem (Chuck *et al.* 1998). A previous fine-mapping study of KRN using a maize–teosinte BC_2S_3 RIL population also identified *ids1* as a strong candidate for KRN (Calderón *et al.* 2016). *unbranched3* (*ub3*) was included within QTL *KRN4.2*, which is an SBP transcription factor that has been shown to regulate KRN in both mutant and QTL studies (Chuck *et al.* 2014; Liu *et al.* 2015). *ramosa1* (*ra1*) was included within *KRN7.1*, which is a C2H2 zinc finger transcription factor controlling inflorescence architecture (Vollbrecht *et al.* 2005).

REPE, which concerns a reddish–brownish pericarp, is a trait that distinguishes teosinte kernels from those of most maize. The role of pigmentation in domestication is complex in that pigments can provide defenses against molding and bird predation, but can also impart bitterness and astringency (Morohashi *et al.* 2012). The red (or reddish–brownish) pigmentation often results from the accumulation of phlobaphenes, which are flavonoid pigments (Morohashi *et al.* 2012). In the absence of the reddish–brownish pigment, the kernels are white unless anthocyanins (blue–purple) or carotenoids (yellow–orange) are present. Our results show that *Pericarp color1* (*P1*) was included within QTL *REPE1.1* (Figure S37), which encodes an R2R3 Myb-like transcription factor that governs the biosynthesis of brick-red flavonoid pigments (Grotewold *et al.* 1994).

Results for 13 additional traits (ASI, BARE, CULM, DTS, EB, ED, EL, GLCO, KW, LFLN, LFWD, PLHT, and YEPE) are reported in the supplemental figures and tables (Figures S30 and S38–S49, and Table S1).

New discoveries and avenues for future research

QTL hotspots: To evaluate whether QTL detected in TeoNAM are overrepresented in specific genomic regions, we counted and plotted the number of QTL peaks using sliding windows of 10- and 1-cM steps (Figure 1). The windows with at least five QTL were considered as QTL hotspots under 1000 permutation tests ($P < 0.001$) and continuous windows were merged together. We totally identified 15 QTL hotspots, ranging from 5 to 13 QTL (Table S4). The two largest hotspots (hs10-1 and hs4-1) were located on chromosomes 10 and 4, respectively. A close view of genes under the hotspots shows that hs10-1

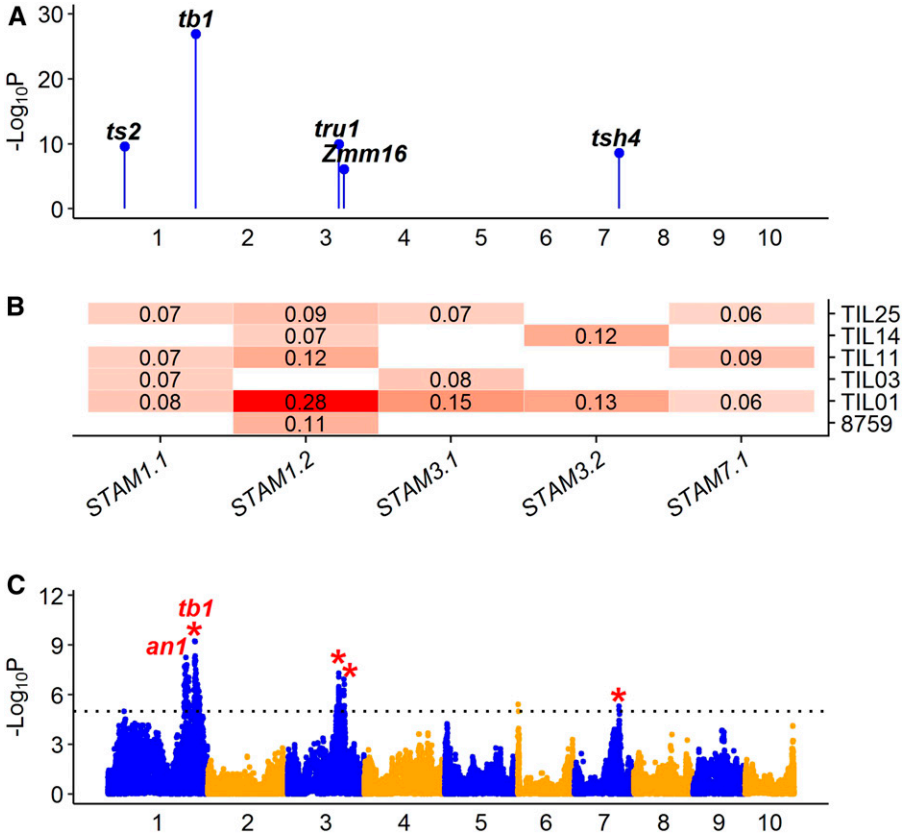

Figure 4 QTL characterization for domestication trait STAM. (A) Genomic distribution of five QTL for STAM detected by JLM. The known candidate genes are shown above the corresponding QTL in bold italic. (B) Heat map shows additive allele effects of teosinte relative to maize for five QTL detected by JLM. The allele effect of teosinte parent 8759 was estimated from the 866 maize–teosinte BC_2S_3 RILs (Shannon 2012). Insignificant effects are shown as blank. The teosinte genotypes at all QTL consistently contribute to a staminate lateral inflorescence. (C) Manhattan plot shows QTL detected by GWAS. The significance threshold at LOD = 5 is indicated by black dotted line. The red stars indicate GWAS signals overlapping with QTL by JLM. In (A) and (C), odd and even numbered chromosomes are shown in blue and orange colors, respectively. GWAS, genome-wide association study; JLM, joint linkage mapping; RIL, recombinant inbred line; STAM, staminate spikelet.

and hs4-1 are around *ZmCCT10* and *tga1*, respectively. These results suggest that these two regulatory genes may have pleiotropic effects on multiple traits.

QTL detection and effects: To evaluate the power of QTL mapping using TeoNAM, we summarized the distribution of QTL detected with significant effects in the different subpopulations. Among 255 QTL for 22 traits, 246 QTL (96%) were detected in two or more subpopulations, 186 QTL (73%) were detected in three or more subpopulations, 83 QTL (33%) were detected in four or more subpopulations, and 29 QTL (11%) were detected in all five subpopulations (Figure 5A). These percentages are conservative as not all traits were scored in all five subpopulations. If one considers whether the QTL was detected in subpopulations in which it was scored, then 205 QTL (80%) were detected in at least one-half of the subpopulations and 39 QTL (15%) were detected in all subpopulations.

The allelic effects from different teosinte parents were estimated simultaneously by JLM. For most QTL, the allelic effects from different subpopulations are in the same direction (Figure 5B). For seven traits (EB, GLUM, LFWD, PROL, SHN, STAM, and YEPE), the teosinte genotypes were consistently associated with a teosinte phenotype and the W22 allele with a maize phenotype at all QTL. For all other traits, there were cases in which a teosinte allele was associated with the maize phenotype. For example, the teosinte genotype is associated with late flowering at most QTL for DTA except *DTA5.2* and *DTA7.1*, for which the teosinte genotype consistently contributes to early flowering in at least three subpopulations (Figure 2). Similar results were observed for KRN and EL. The teosinte genotype is associated with lower KRN at most QTL, but there is one QTL (*KRN5.1*) for which the teosinte genotype is consistently associated with higher KRN in four subpopulations and also in the BC_2S_3 population (Figure S36). The teosinte genotype is associated with shorter EL at most QTL, but there are two QTL (*EL4.1* and *EL9.1*) for which the teosinte genotype is consistently associated with longer EL in four and two subpopulations, respectively (Figure S43). These QTL might be worth exploring further for use in maize improvement.

We also observed notable results for different teosinte parents. For KW, the teosinte genotype from different subpopulations is associated with reduced kernel weight at most QTL. Only three QTL (*KW5.3*, *KW6.2*, and *KW9.1*) are exceptions, with one teosinte allele conferring heavier kernels. Interestingly, for these three QTL, the teosinte alleles with effects in the opposite direction are all from the TIL14 subpopulation (Figure S45). Similar results were observed for ED, where the teosinte genotype is associated with a decrease in ED at most QTL, but the teosinte allele from TIL03 at two QTL (*ED2.1* and *ED6.1*) is associated with the increase of ED (Figure S42). These results suggest that there are beneficial alleles from teosinte that could be utilized for maize improvement.

Comparing and combining TeoNAM with BC_2S_3: We compared TeoNAM with our previous maize–teosinte BC_2S_3 RIL

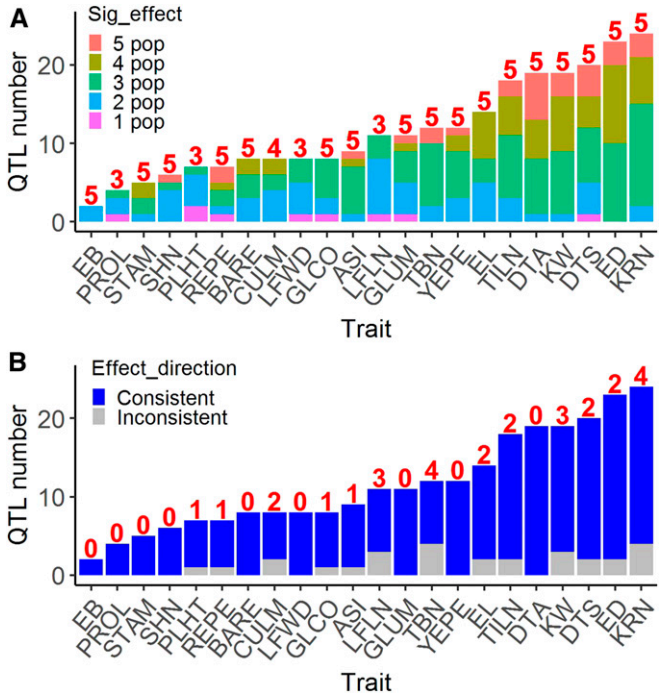

Figure 5 QTL detection and effects for all 22 traits. (A) Summary of QTL detection for all 22 traits. The number above the bar indicates the number of subpopulations in which the trait was scored. (B) Summary of QTL effect directions for all 22 traits. The number above the bar indicates the number of QTL within which a teosinte allele associated with the maize phenotype was detected.

population. The composite genetic map for TeoNAM is 1540 cM in length. The individual genetic maps based on the five subpopulations have an average length of 1461 cM with a range of 1348–1596 cM. The genetic map for BC_2S_3 RIL population is 1478 cM in length. Thus, the TeoNAM subpopulations are similar to the BC_2S_3 RIL population in genetic map length. The median length of homozygous teosinte segments in TeoNAM is 7.5 Mb. The median length of homozygous teosinte segments in BC_2S_3 population is 4.8 Mb. The longer segment length for TeoNAM is expected given it had one fewer generations of backcrossing and less opportunity for recombination. The mean number of homozygous teosinte segments in TeoNAM is 2414 and the number of homozygous teosinte segments in BC_2S_3 is 5745. The total length of teosinte segments for the five subpopulations is 67 gigabases (Gb) (W22 × TIL01), 87 Gb (W22 × TIL03), 66 Gb (W22 × TIL11), 59 Gb (W22 × TIL14), and 79 Gb (W22 × TIL25), and BC_2S_3 (W22 × 8759) exceeds this range with 110 Gb.

Previously, Shannon (2012) performed a comprehensive interval QTL analysis for 16 agronomic traits in the BC_2S_3 population and identified 218 QTL for 16 traits. Among these traits, 14 traits were also scored in TeoNAM population. For the common 14 traits, 168 and 179 QTL were detected for the TeoNAM and BC_2S_3 populations, respectively. The mean 1.5-LOD QTL support interval across 14 traits for BC_2S_3 is 5.7 Mb, which is significantly smaller than the TeoNAM interval of 17.2 Mb determined by JLM (P = 2.6E–08) (Figure S50). Among these QTL, 50 overlapped between the two populations. For the common QTL, the mean variance explained by QTL is 3.4 and 2.9% for BC_2S_3 and TeoNAM, respectively. Thus, there is no significant difference in QTL effect size (P = 0.3) (Figure S51).

Among the 50 common QTL between TeoNAM and BC_2S_3, 12 QTL were detected with significant effects and consistent effect directions in all five subpopulations of TeoNAM and BC_2S_3 (Table 3). Another 23 QTL were not significant in all five subpopulations of TeoNAM but with consistent effect direction (Table 3). Among these QTL, known candidates include *zagl1* for *DTA1.1*, *Zmm31* for *DTA5.1*, *dlf1* for *DTA7.2*, *ZCN8* for *DTA8.1*, *ZmCCT9* for *DTA9.1*, *ZmCCT10* for *DTA10.1*, *tga1* for *GLUM4.1*, *ids1* for *KRN1.3*, *ra1* for *KRN7.1*, *P1* for *REPE1.1*, *ZmSh1-1* for *SHN1.1*, *ZAG2* for *TILN3.2*, and *tb1* for *ED1.3* and *STAM1.2*. There are also novel candidates: *smk1* (*small kernel1*) for *ED2.4* and *GIF1* (*GRAIN INCOMPLETE FILLING 1*) for *EL10.1*. *smk1* encodes a pentatricopeptide repeat protein required for mitochondrial *nad7* (*NADH dehydrogenase subunit7*) transcript editing, and seed development in maize and rice (Li *et al.* 2014). *GIF1* encodes a cell wall invertase required for carbon partitioning during early grain filling in rice (Wang *et al.* 2008). Among the candidates, causative sites have been reported for only three: *ZCN8*, *ZmCCT10*, and *tga1*. Therefore, there are many new candidates for future fine-mapping of their causative polymorphisms.

To maximize the power to detect QTL, we combined TeoNAM and BC_2S_3 for eight traits (DTA, ED, EL, KRN, KW, GLCO, GLUM, and TILN) that were measured in all six subpopulations via the exact same method used to perform JLM. Before analysis, we imputed the genotype for BC_2S_3 at 4578 TeoNAM SNPs according to the flanking markers using the same procedure as for TeoNAM and permuted a new P-value cutoff for statistical significance for each trait. The Least Squared Means (LSMs) from previous analysis (Shannon 2012) were used for JLM. With the combined TeoNAM–BC_2S_3 data, we detected 184 QTL for these eight traits, which included 109 QTL overlapping with TeoNAM, 80 QTL overlapping with the BC_2S_3, and 32 novel QTL that were not detected in either TeoNAM or BC_2S_3 (Table S5). The QTL with significant allele effects in multiple subpopulations will be good targets for fine-mapping. For future analysis of additional traits, one could combine TeoNAM and the BC_2S_3 together. The value of this combination is that there is one additional teosinte allele and increased QTL detection power, but the downside is that one would need to assay the BC_2S_3 population using 866 RILs plus TeoNAM with 1257 RILs.

Discussion

RILs are powerful tools for dissecting the complex genetic architectures of different traits and for gene discovery. RILs such as the maize NAM population have been successfully used for the genetic dissection of many traits (Buckler *et al.* 2009; Kump *et al.* 2011; Tian *et al.* 2011). RILs with multiple

Table 3 QTL with same effect direction between TeoNAM and BC_2S_3

Trait	QTL	Chr	QTL peak (V4) (Mb)	Support interval (V4) (Mb)	QTL peak (cM)	Support interval (cM)	*P*-value	TIL01	TIL03	TIL11	TIL14	TIL25	8759[a]	Candidate gene
BARE	*BARE4.3*	4	55.9	39.0–124.3	61.5	58.2–66.8	4.72E–07	0.19	0.25	0.19	0.14[b]	0.09[b]	0.63	*tga1*
DTA	*DTA1.1*	1	4.5	2.8–5.6	9.0	3.4–13.2	1.26E–16	0.59	1.02	1.23	1.31	0.77	0.81	*zagl1*
DTA	*DTA3.3*	3	231.4	226.3–233.4	167.2	156.7–170.0	4.54E–08	0.64	1.05	0.68	0.13[b]	0.73	0.49	
DTA	*DTA5.1*	5	6.9	6.7–7.2	30.7	29.2–31.5	2.62E–18	1.11	0.80	1.11	1.24	1.30	0.66	*Zmm31*
DTA	*DTA7.2*	7	180.4	180.1–180.8	140.7	139.3–141.8	2.92E–14	0.53	1.37	0.77	0.58	1.16	0.59	*dlf1*
DTA	*DTA8.1*	8	126.9	126.6–126.9	68.3	68.2–68.3	4.05E–54	1.64	2.00	2.63	1.72	1.59	1.54	*ZCN8*
DTA	*DTA9.1*	9	117.5	115.7–118.8	72.9	72.4–74.6	4.76E–33	0.65	3.16	1.24	0.74	1.39	0.79	*ZmCCT9*
DTA	*DTA10.1*	10	95.4	94.9–99.4	54.7	54.3–55.1	9.29E–121	3.47	3.22	2.46	4.87	4.54	3.61	*ZmCCT10*
EB	*EB7.1*	7	121.5	103.9–132.7	64.8	60.1–72.7	5.18E–14	0.02[b]	0.01[b]	0.06	0.05	0.01[b]	0.05	
ED	*ED1.3*	1	277.1	265.1–283.1	134.7	127.6–141.3	6.45E–06	−1.02	−0.28[b]	−1.38	−0.25[b]	−0.64	−1.87	*tb1*
ED	*ED2.4*	2	217.2	211.9–223.4	123.3	116.8–133.5	1.22E–06	−0.46[b]	−0.79	−0.39[b]	−0.72	−0.85	−0.88	*smk1*
ED	*ED3.2*	3	218.4	214.8–219.8	140.1	133.8–142.3	1.34E–13	−1.18	−0.45	−0.72	−0.34[b]	−1.33	−0.89	
ED	*ED4.1*	4	7.8	6.8–11.1	23.8	21.5–30.1	1.50E–11	−1.59	−0.48	−0.01[b]	−0.64	−0.25[b]	−0.74	
ED	*ED7.2*	7	163.6	160.4–164.2	98.0	94.1–98.4	2.47E–19	−0.67	−0.94	−1.59	−1.30	−0.78	−0.81	
EL	*EL7.1*	7	125.5	123.7–130.3	66.8	65.7–70.5	4.64E–17	−0.82	−0.34	−0.56	−0.21[b]	−0.81	−0.97	
EL	*EL8.1*	8	156.5	150.4–157.6	82.5	78.1–83.4	2.84E–11	−0.19[b]	−0.48	−0.15[b]	−0.21[b]	−0.68	−0.66	
EL	*EL10.1*	10	115.0	115.0–118.9	58.5	58.8–60.0	6.87E–40	−0.12[b]	−0.88	−0.85	−1.68	−1.17	−1.34	*GIF1*
GLCO	*GLCO4.1*	4	42.1	39.0–42.1	59.6	58.2–59.6	5.98E–24	0.01[b]	0.12	0.08[b]	0.31	0.37	0.27	
GLUM	*GLUM4.1*	4	42.1	40.4–55.9	59.6	59.1–61.5	2.57E–168	0.74	0.77	0.73	0.93	1.06	0.8	*tga1*
KRN	*KRN1.3*	1	298.5	298.1–299.6	165.7	164.9–168.2	2.73E–16	−0.51	−0.58	−0.35	−0.09[b]	−0.26	−0.63	*ids1*
KRN	*KRN4.3*	4	243.5	241.6–244.8	145.6	137.4–152.1	8.27E–07	−0.22	−0.41	−0.18	−0.23	−0.23	−0.55	
KRN	*KRN5.1*	5	2.4	2.3–2.9	12.7	11.7–15.0	8.72E–14	0.36	0.51	0.12[b]	0.40	0.24	0.3	
KRN	*KRN7.1*	7	95.2	21.5–123.7	58.6	49.6–65.7	7.00E–11	−0.36	−0.18	−0.54	−0.06[b]	−0.42	−0.26	*ra1*
KRN	*KRN8.2*	8	171.3	169.6–173.4	106.8	100.8–113.0	6.70E–13	−0.49	−0.40	−0.38	−0.04[b]	−0.15[b]	−0.25	
KW	*KW1.2*	1	234.3	222.8–252.5	110.3	106.5–116.4	6.01E–10	−0.01	−0.01	−0.01	−0.00[b]	−0.01	−0.01	
KW	*KW2.1*	2	53.3	36.9–57.5	74.3	64.3–76.1	1.32E–11	−0.01	−0.00[b]	−0.01	−0.01	−0.00[b]	−0.01	
KW	*KW4.2*	4	170.1	156.8–174.8	82.8	73.6–84.2	1.69E–08	−0.01	−0.01	−0.01	−0.00[b]	−0.00[b]	−0.01	
KW	*KW8.1*	8	137.7	132.5–145.9	72.7	70.4–75.4	1.31E–12	−0.00[b]	−0.01	−0.01	−0.01	−0.01	−0.01	
REPE	*REPE1.1*	1	47.0	46.5–51.8	64.9	64.4–68.3	2.71E–11	−0.10	−0.10	−0.06	−0.10	−0.10	−0.10	*P1*
SHN	*SHN1.1*	1	265.1	264.1–265.1	127.6	127.2–127.6	3.21E–16	0.08	0.09	0.18	0.17	0.11	0.07	*ZmSh1-1*
SHN	*SHN6.1*	6	162.5	162.2–163.6	98.2	97.4–101.1	3.49E–11	0.06	0.04[b]	0.17	0.03[b]	0.10	0.06	
STAM	*STAM1.2*	1	270.5	269.8–270.5	130.2	129.5–130.2	1.23E–27	0.28	0.02[b]	0.12	0.07	0.09	0.11	*tb1*
TILN	*TILN3.2*	3	138.3	137.6–158.6	80.5	80.2–86.2	5.22E–24	0.00[b]	0.42	0.33	0.08[b]	0.20	0.14	*ZAG2*
TILN	*TILN5.1*	5	69.0	36.0–140.7	75.4	69.9–82.7	6.66E–10	0.18	0.24	0.14	0.14	0.16	0.10	
TILN	*TILN10.1*	10	62.5	25.3–82.1	47.7	45.0–51.1	4.10E–13	0.15	0.24	0.06[b]	0.08[b]	0.28	0.12	

BARE, barren ear base; DTA, days to anthesis; EB, ear branch number; ED, ear diameter; EL, ear length; GLCO, glume color; GLUM, glume score; KRN, kernel row number; KW, kernel weight; REPE, red pericarp; SHN, shattering; STAM, staminate spikelet; TILN, tiller number. Chr, chromosome; JLM, joint linkage mapping; TeoNAM, teosinte nested association mapping.

[a] The allele effect of 8759 relative to maize was estimated in BC_2S_3 by Shannon (2012).

[b] Indicates that the additive allele effect of teosinte relative to maize estimated from JLM in TeoNAM is not significant.

parents greatly increase the power and precision to identify QTL compared to the traditional biparent RIL population. Multiparent RILs also enable the estimation of allele effects simultaneously from each inbred parent. Our TeoNAM RILs were created by crossing five teosinte inbred parents with a maize inbred parent, but differ from MaizeNAM in that we applied a generation of backcrossing to the maize parent before four generations of selfing. The power and precision of TeoNAM can be shown with several traits. For example, we detected 19 QTL for DTA, among which many QTL mapped to recently cloned genes such as *ZmCCT10*, *ZmCCT9*, *ZCN8*, *zagl1*, and *ZmMADS69*. QTL also mapped to some novel candidates such as *dlf1*, *si1*, *ZAG1*, *ZCN12*, *Zmm19*, and *Zmm31*, which may have an important role in flowering time regulation.

For RIL populations, both JLM and GWAS are common methods for QTL detection. In this study, we identified 255 QTL for 22 traits by JLM, and significant peaks were detected at 57 QTL by GWAS, which suggests that GWAS is less powerful than JLM for mapping QTL in TeoNAM. Nevertheless, there were a few instances in which GWAS gave evidence of closely linked QTL that were not separated by JLM. For example, we did not identify *an1*, a strong candidate for STAM QTL on chromosome 1, with JLM possibly because it is closely linked to *tb1* (candidate of QTL *STAM1.2*), but we detected distinct and significant peaks at both *an1* and *tb1* through GWAS as it tests each SNP independently.

TeoNAM reveals that there are distinct genetic architectures for different traits. Traits like PROL and GLUM are controlled by a major effect QTL plus several QTL of very small effect, while traits like DTA and KRN show more classic polygenic inheritance. Domestication traits controlled by single major genes have frequently been reported in a variety of crops (Doebley *et al.* 2006). There is less emphasis in the literature on

polygenic inheritance of domestication traits, although a well-known example is fruit size in tomato (Frary *et al.* 2000). Our results highlight the importance of these two modes of inheritance during the domestication process.

A relatively large phenotypic data set of 22 traits scored in TeoNAM allowed us to evaluate QTL hotspots. We detected 15 QTL hotspots, in which the largest hotspot could affect 13 traits. However, this should be treated with caution regard whether these hotspots were caused by a single master gene with pleiotropic effects or several genes that are tightly linked together, as domestication may favor the selection of tightly linked combinations of genes (Le Thierry d'Ennequin *et al.* 1999).

In our study, a total of 15 domestication traits and 7 agronomic traits were analyzed. Further fine-mapping and gene cloning will be required to find the causal genes underlying QTL for these traits. TeoNAM should also be useful for investigating the genetic control of many new traits that we did not assay. Morphological traits such as root architecture, shoot apical meristem size, vasculature, pollen size, and kernel shape can be explored. Also, molecular traits such as gene expression (eQTL) (Wang *et al*. 2018), alternative splicing (Chen *et al*. 2018), grain protein content (Cook *et al*. 2012), and metabolites (Xu *et al*. 2019) can also be explored to better understand the full spectrum of changes that occurred during maize domestication. In this context, we note that TeoNAM was developed as part of an undergraduate research project and phenotyping performed over three field seasons, but the entire set of lines was never grown in a single season. Increased power beyond that which we report here can be gained by growing the entire set of lines each season for multiple seasons to obtain better phenotypic data, and more power in QTL detection.

Acknowledgments

We thank Karl Broman for suggestions on the analyses and Jesse Rucker, Elizabeth Buschert, Eric Rentmeester, Adam Mittermaier, David Sierakowski, and Brian Schaeffer for assistance with field work and phenotyping. This research was supported by the US National Science Foundation (grant IOS 1238014) and the China Postdoctoral Science Foundation (2018M640204).

Literature Cited

Ambrose, B. A., D. R. Lerner, P. Ciceri, C. M. Padilla, M. F. Yanofsky *et al*., 2000 Molecular and genetic analyses of the *silky1* gene reveal conservation in floral organ specification between eudicots and monocots. Mol. Cell 5: 569–579. https://doi.org/10.1016/S1097-2765(00)80450-5

Bandillo, N., C. Raghavan, P. A. Muyco, M. A. Sevilla, I. T. Lobina *et al*., 2013 Multi-parent advanced generation inter-cross (MAGIC) populations in rice: progress and potential for genetics research and breeding. Rice (N Y) 6: 11. https://doi.org/10.1186/1939-8433-6-11

Barazesh, S., and P. McSteen, 2008 *Barren inflorescence1* functions in organogenesis during vegetative and inflorescence development in maize. Genetics 179: 389–401. https://doi.org/10.1534/genetics.107.084079

Bensen, R. J., G. S. Johal, V. C. Crane, J. T. Tossberg, P. S. Schnable *et al*., 1995 Cloning and characterization of the maize *An1* gene. Plant Cell 7: 75–84. https://doi.org/10.1105/tpc.7.1.75

Bomblies, K., R. L. Wang, B. A. Ambrose, R. J. Schmidt, R. B. Meeley *et al*., 2003 Duplicate *FLORICAULA/LEAFY* homologs *zfl1* and *zfl2* control inflorescence architecture and flower patterning in maize. Development 130: 2385–2395. https://doi.org/10.1242/dev.00457

Bouchet, S., M. O. Olatoye, S. R. Marla, R. Perumal, and T. Tesso, 2017 Increased power to dissect adaptive traits in global sorghum diversity using a nested association mapping population. Genetics 206: 573–585. https://doi.org/10.1534/genetics.116.198499

Bradbury, P. J., Z. Zhang, D. E. Kroon, T. M. Casstevens, Y. Ramdoss *et al*., 2007 TASSEL: software for association mapping of complex traits in diverse samples. Bioinformatics 23: 2633–2635. https://doi.org/10.1093/bioinformatics/btm308

Broman, K. W., H. Wu, Ś. Sen, and G. A. Churchill, 2003 R/qtl: QTL mapping in experimental crosses. Bioinformatics 19: 889–890. https://doi.org/10.1093/bioinformatics/btg112

Buckler, E. S., J. B. Holland, P. J. Bradbury, C. B. Acharya, P. J. Brown *et al*., 2009 The genetic architecture of maize flowering time. Science 325: 714–718. https://doi.org/10.1126/science.1174276

Calderón, C. I., B. S. Yandell, and J. F. Doebley, 2016 Fine mapping of a QTL associated with kernel row number on chromosome 1 of maize. PLoS One 11: e0150276. https://doi.org/10.1371/journal.pone.0150276

Chen, Q., Y. Han, H. Liu, X. Wang, J. Sun *et al*., 2018 Genome-wide association analyses reveal the importance of alternative splicing in diversifying gene function and regulating phenotypic variation in maize. Plant Cell 30: 1404–1423. https://doi.org/10.1105/tpc.18.00109

Chuck, G., R. B. Meeley, and S. Hake, 1998 The control of maize spikelet meristem fate by the *APETALA2*-like gene *indeterminate spikelet1*. Genes Dev. 12: 1145–1154. https://doi.org/10.1101/gad.12.8.1145

Chuck, G., C. Whipple, D. Jackson, and S. Hake, 2010 The maize SBP-box transcription factor encoded by *tasselsheath4* regulates bract development and the establishment of meristem boundaries. Development 137: 1243–1250. https://doi.org/10.1242/dev.048348

Chuck, G. S., P. J. Brown, R. Meeley, and S. Hake, 2014 Maize *SBP-box* transcription factors *unbranched2* and *unbranched3* affect yield traits by regulating the rate of lateral primordia initiation. Proc. Natl. Acad. Sci. USA 111: 18775–18780. https://doi.org/10.1073/pnas.1407401112

Churchill, G. A., D. C. Airey, H. Allayee, J. M. Angel, A. D. Attie *et al*., 2004 The collaborative cross, a community resource for the genetic analysis of complex traits. Nat. Genet. 36: 1133–1137. https://doi.org/10.1038/ng1104-1133

Cook, J. P., M. D. McMullen, J. B. Holland, F. Tian, P. Bradbury *et al*., 2012 Genetic architecture of maize kernel composition in the nested association mapping and inbred association panels. Plant Physiol. 158: 824–834. https://doi.org/10.1104/pp.111.185033

Dell'Acqua, M., D. M. Gatti, G. Pea, F. Cattonaro, F. Coppens *et al*., 2015 Genetic properties of the MAGIC maize population: a new platform for high definition QTL mapping in *Zea mays*. Genome Biol. 16: 167. https://doi.org/10.1186/s13059-015-0716-z

Doebley, J., A. Stec, and C. Gustus, 1995 *Teosinte branched1* and the origin of maize: evidence for epistasis and the evolution of dominance. Genetics 141: 333–346.

Doebley, J., A. Stec, and L. Hubbard, 1997 The evolution of apical dominance in maize. Nature 386: 485–488. https://doi.org/10.1038/386485a0

Doebley, J. F., B. S. Gaut, and B. D. Smith, 2006 The molecular genetics of crop domestication. Cell 127: 1309–1321. https://doi.org/10.1016/j.cell.2006.12.006

Dong, Z., W. Li, E. Unger-Wallace, J. Yang, E. Vollbrecht *et al.*, 2017 Ideal crop plant architecture is mediated by *tassels replace upper ears1*, a BTB/POZ ankyrin repeat gene directly targeted by TEOSINTE BRANCHED1. Proc. Natl. Acad. Sci. USA 114: E8656–E8664. https://doi.org/10.1073/pnas.1714960114

Elshire, R. J., J. C. Glaubitz, Q. Sun, J. A. Poland, K. Kawamoto *et al.*, 2011 A robust, simple genotyping-by-sequencing (GBS) approach for high diversity species. PLoS One 6: e19379. https://doi.org/10.1371/journal.pone.0019379

Fragoso, C. A., M. Moreno, Z. Wang, C. Heffelfinger, L. J. Arbelaez *et al.*, 2017 Genetic architecture of a rice nested association mapping population. G3 (Bethesda) 7: 1913–1926. https://doi.org/10.1534/g3.117.041608

Frary, A., T. C. Nesbitt, A. Frary, S. Grandillo, E. Van Der Knaap *et al.*, 2000 *fw2. 2*: a quantitative trait locus key to the evolution of tomato fruit size. Science 289: 85–88. https://doi.org/10.1126/science.289.5476.85

Fu, Y., G. Xu, H. Chen, X. Wang, Q. Chen *et al.*, 2019 QTL mapping for leaf morphology traits in a large maize-teosinte population. Mol. Breed. 39: 103. https://doi.org/10.1007/s11032-019-1012-5

Gallavotti, A., S. Barazesh, S. Malcomber, D. Hall, D. Jackson *et al.*, 2008 *Sparse inflorescence1* encodes a monocot-specific *YUCCA*-like gene required for vegetative and reproductive development in maize. Proc. Natl. Acad. Sci. USA 105: 15196–15201. https://doi.org/10.1073/pnas.0805596105

Glaubitz, J. C., T. M. Casstevens, F. Lu, J. Harriman, R. J. Elshire *et al.*, 2014 TASSEL-GBS: a high capacity genotyping by sequencing analysis pipeline. PLoS One 9: e90346. https://doi.org/10.1371/journal.pone.0090346

Grotewold, E., B. J. Drummond, B. Bowen, and T. Peterson, 1994 The *myb*-homologous *P* gene controls phlobaphene pigmentation in maize floral organs by directly activating a flavonoid biosynthetic gene subset. Cell 76: 543–553. https://doi.org/10.1016/0092-8674(94)90117-1

Guo, L., X. Wang, M. Zhao, C. Huang, C. Li *et al.*, 2018 Stepwise *cis*-regulatory changes in *ZCN8* contribute to maize flowering-time adaptation. Curr. Biol. 28: 3005–3015.e4. https://doi.org/10.1016/j.cub.2018.07.029

Huang, B. E., A. W. George, K. L. Forrest, A. Kilian, M. J. Hayden *et al.*, 2012 A multiparent advanced generation inter-cross population for genetic analysis in wheat. Plant Biotechnol. J. 10: 826–839. https://doi.org/10.1111/j.1467-7652.2012.00702.x

Huang, C., Q. Chen, G. Xu, D. Xu, J. Tian *et al.*, 2016 Identification and fine mapping of quantitative trait loci for the number of vascular bundle in maize stem. J. Integr. Plant Biol. 58: 81–90. https://doi.org/10.1111/jipb.12358

Huang, C., H. Sun, D. Xu, Q. Chen, Y. Liang *et al.*, 2018 *ZmCCT9* enhances maize adaptation to higher latitudes. Proc. Natl. Acad. Sci. USA 115: E334–E341. https://doi.org/10.1073/pnas.1718058115

Huang, X., M. J. Paulo, M. Boer, S. Effgen, P. Keizer, M. Koornneef *et al.*, 2011 Analysis of natural allelic variation in *Arabidopsis* using a multiparent recombinant inbred line population. Proc. Natl. Acad. Sci. USA 108: 4488–4493. https://doi.org/10.1073/pnas.1100465108

Hung, H.-Y., L. M. Shannon, F. Tian, P. J. Bradbury, C. Chen *et al.*, 2012 *ZmCCT* and the genetic basis of day-length adaptation underlying the postdomestication spread of maize. Proc. Natl. Acad. Sci. USA 109: E1913–E1921. https://doi.org/10.1073/pnas.1203189109

Irish, E. E., and T. M. Nelson, 1993 Development of *tassel seed 2* inflorescences in maize. Am. J. Bot. 80: 292–299. https://doi.org/10.1002/j.1537-2197.1993.tb13802.x

Jin, J., W. Huang, J. P. Gao, J. Yang, M. Shi *et al.*, 2008 Genetic control of rice plant architecture under domestication. Nat. Genet. 40: 1365–1369. https://doi.org/10.1038/ng.247

Jordan, K. W., S. Wang, F. He, S. Chao, Y. Lun *et al.*, 2018 The genetic architecture of genome-wide recombination rate variation in allopolyploid wheat revealed by nested association mapping. Plant J. 95: 1039–1054. https://doi.org/10.1111/tpj.14009

King, E. G., C. M. Merkes, C. L. McNeil, S. R. Hoofer, S. Sen *et al.*, 2012 Genetic dissection of a model complex trait using the *Drosophila* Synthetic Population Resource. Genome Res. 22: 1558–1566. https://doi.org/10.1101/gr.134031.111

Kover, P. X., W. Valdar, J. Trakalo, N. Scarcelli, I. M. Ehrenreich *et al.*, 2009 A multiparent advanced generation inter-cross to fine-map quantitative traits in *Arabidopsis thaliana*. PLoS Genet. 5: e1000551. https://doi.org/10.1371/journal.pgen.1000551

Kremling, K. A., S. Y. Chen, M. H. Su, N. K. Lepak, M. C. Romay *et al.*, 2018 Dysregulation of expression correlates with rare-allele burden and fitness loss in maize. Nature 555: 520–523. https://doi.org/10.1038/nature25966

Kump, K. L., P. J. Bradbury, R. J. Wisser, E. S. Buckler, A. R. Belcher *et al.*, 2011 Genome-wide association study of quantitative resistance to southern leaf blight in the maize nested association mapping population. Nat. Genet. 43: 163–168. https://doi.org/10.1038/ng.747

Lang, Z., D. M. Wills, Z. H. Lemmon, L. M. Shannon, R. Bukowski *et al.*, 2014 Defining the role of *prolamin-box binding factor1* gene during maize domestication. J. Hered. 105: 576–582. https://doi.org/10.1093/jhered/esu019

Leiboff, S., C. K. DeAllie, and M. J. Scanlon, 2016 Modeling the morphometric evolution of the maize shoot apical meristem. Front. Plant Sci. 7: 1651. https://doi.org/10.3389/fpls.2016.01651

Le Thierry d'Ennequin, M., B. Toupance, T. Robert, B. Godelle, and P. Gouyon, 1999 Plant domestication: a model for studying the selection of linkage. J. Evol. Biol. 12: 1138–1147. https://doi.org/10.1046/j.1420-9101.1999.00115.x

Li, D., X. Wang, X. Zhang, Q. Chen, G. Xu *et al.*, 2016 The genetic architecture of leaf number and its genetic relationship to flowering time in maize. New Phytol. 210: 256–268. https://doi.org/10.1111/nph.13765

Li, X. J., Y. F. Zhang, M. Hou, F. Sun, Y. Shen *et al.*, 2014 *Small kernel 1* encodes a pentatricopeptide repeat protein required for mitochondrial *nad7* transcript editing and seed development in maize (*Zea mays*) and rice (*Oryza sativa*). Plant J. 79: 797–809. https://doi.org/10.1111/tpj.12584

Liang, Y., Q. Liu, X. Wang, C. Huang, G. Xu *et al.*, 2019 *ZmMADS69* functions as a flowering activator through the *ZmRap2.7-ZCN8* regulatory module and contributes to maize flowering time adaptation. New Phytol. 221: 2335–2347. https://doi.org/10.1111/nph.15512

Lin, Z., X. Li, L. M. Shannon, C. T. Yeh, M. L. Wang *et al.*, 2012 Parallel domestication of the *Shattering1* genes in cereals. Nat. Genet. 44: 720–724. https://doi.org/10.1038/ng.2281

Liu, L., Y. Du, X. Shen, M. Li, W. Sun *et al.*, 2015 *KRN4* controls quantitative variation in maize kernel row number. PLoS Genet. 11: e1005670. https://doi.org/10.1371/journal.pgen.1005670

Mackay, I. J., P. Bansept-Basler, T. Barber, A. R. Bentley, J. Cockram *et al.*, 2014 An eight-parent multiparent advanced generation inter-cross population for winter-sown wheat: creation, properties, and validation. G3 (Bethesda) 4: 1603–1610. https://doi.org/10.1534/g3.114.012963

Maurer, A., V. Draba, Y. Jiang, F. Schnaithmann, R. Sharma *et al.*, 2015 Modelling the genetic architecture of flowering time control in barley through nested association mapping. BMC Genomics 16: 290. https://doi.org/10.1186/s12864-015-1459-7

Meng, X., M. G. Muszynski, and O. N. Danilevskaya, 2011 The *FT*-like *ZCN8* gene functions as a floral activator and is involved in photoperiod sensitivity in maize. Plant Cell 23: 942–960. https://doi.org/10.1105/tpc.110.081406

Morohashi, K., M. I. Casas, M. L. Falcone Ferreyra, M. K. Mejía-Guerra, L. Pourcel *et al.*, 2012 A genome-wide regulatory framework identifies maize *Pericarp Color1* controlled genes. Plant Cell 24: 2745–2764 (erratum: Plant Cell 24: 3853). https://doi.org/10.1105/tpc.112.098004

Nice, L. M., B. J. Steffenson, G. L. Brown-Guedira, E. D. Akhunov, C. Liu *et al.*, 2016 Development and genetic characterization of an advanced backcross-nested association mapping (AB-NAM) population of wild × cultivated barley. Genetics 203: 1453–1467. https://doi.org/10.1534/genetics.116.190736

Pautler, M., A. L. Eveland, T. LaRue, F. Yang, R. Weeks *et al.*, 2015 *FASCIATED EAR4* encodes a bZIP transcription factor that regulates shoot meristem size in maize. Plant Cell 27: 104–120. https://doi.org/10.1105/tpc.114.132506

Schmidt, R. J., B. Veit, M. A. Mandel, M. Mena, S. Hake *et al.*, 1993 Identification and molecular characterization of *ZAG1*, the maize homolog of the Arabidopsis floral homeotic gene *AGAMOUS*. Plant Cell 5: 729–737. https://doi.org/10.1105/tpc.5.7.729

Shannon, L. M., 2012 The genetic architecture of maize domestication and range expansion. Ph.D. Thesis, The University of Wisconsin–Madison, Madison, WI.

Shannon, L. M., Q. Chen, and J. F. Doebley, 2019 A BC_2S_3 maize-teosinte RIL population for QTL mapping. Maize Genet. Coop. News Lett. 93.

Studer, A. J., H. Wang, and J. F. Doebley, 2017 Selection during maize domestication targeted a gene network controlling plant and inflorescence architecture. Genetics 207: 755–765. https://doi.org/10.1534/genetics.117.300071

Tan, L., X. Li, F. Liu, X. Sun, C. Li *et al.*, 2008 Control of a key transition from prostrate to erect growth in rice domestication. Nat. Genet. 40: 1360–1364. https://doi.org/10.1038/ng.197

Theissen, G., A. Becker, A. Di Rosa, A. Kanno, J. T. Kim *et al.*, 2000 A short history of MADS-box genes in plants. Plant Mol. Evol. 42: 115–149. https://doi.org/10.1007/978-94-011-4221-2_6

Tian, F., P. J. Bradbury, P. J. Brown, H. Hung, Q. Sun *et al.*, 2011 Genome-wide association study of leaf architecture in the maize nested association mapping population. Nat. Genet. 43: 159–162. https://doi.org/10.1038/ng.746

Tian, J., C. Wang, J. Xia, L. Wu, G. Xu *et al.*, 2019 Teosinte ligule allele narrows plant architecture and enhances high-density maize yields. Science 365: 658–664. https://doi.org/10.1126/science.aax5482

Vollbrecht, E., P. S. Springer, L. Goh, E. S. Buckler, IV, and R. Martienssen, 2005 Architecture of floral branch systems in maize and related grasses. Nature 436: 1119–1126. https://doi.org/10.1038/nature03892

Wang, E., J. Wang, X. Zhu, W. Hao, L. Wang *et al.*, 2008 Control of rice grain-filling and yield by a gene with a potential signature of domestication. Nat. Genet. 40: 1370–1374. https://doi.org/10.1038/ng.220

Wang, H., T. Nussbaum-Wagler, B. Li, Q. Zhao, Y. Vigouroux *et al.*, 2005 The origin of the naked grains of maize. Nature 436: 714–719. https://doi.org/10.1038/nature03863

Wang, H., A. J. Studer, Q. Zhao, R. Meeley, and J. F. Doebley, 2015 Evidence that the origin of naked kernels during maize domestication was caused by a single amino acid substitution in *tga1*. Genetics 200: 965–974. https://doi.org/10.1534/genetics.115.175752

Wang, X., Q. Chen, Y. Wu, Z. H. Lemmon, G. Xu *et al.*, 2018 Genome-wide analysis of transcriptional variability in a large maize-teosinte population. Mol. Plant 11: 443–459. https://doi.org/10.1016/j.molp.2017.12.011

Whipple, C. J., D. H. Hall, S. DeBlasio, F. Taguchi-Shiobara, R. J. Schmidt *et al.*, 2010 A conserved mechanism of bract suppression in the grass family. Plant Cell 22: 565–578. https://doi.org/10.1105/tpc.109.073536

Whipple, C. J., T. H. Kebrom, A. L. Weber, F. Yang, D. Hall *et al.*, 2011 *grassy tillers1* promotes apical dominance in maize and responds to shade signals in the grasses. Proc. Natl. Acad. Sci. USA 108: E506–E512. https://doi.org/10.1073/pnas.1102819108

Wills, D. M., C. J. Whipple, S. Takuno, L. E. Kursel, L. M. Shannon *et al.*, 2013 From many, one: genetic control of prolificacy during maize domestication. PLoS Genet. 9: e1003604. https://doi.org/10.1371/journal.pgen.1003604

Wills, D. M., Z. Fang, A. M. York, J. B. Holland, and J. F. Doebley, 2017 Defining the role of the MADS-box gene, *Zea Agamous-like1*, a target of selection during maize domestication. J. Hered. 109: 333–338. https://doi.org/10.1093/jhered/esx073

Xavier, A., D. Jarquin, R. Howard, V. Ramasubramanian, J. E. Specht *et al.*, 2018 Genome-wide analysis of grain yield stability and environmental interactions in a multiparental soybean population. G3 (Bethesda) 8: 519–529. https://doi.org/10.1534/g3.117.300300

Xu, D., X. Wang, C. Huang, G. Xu, Y. Liang *et al.*, 2017 *Glossy15* plays an important role in the divergence of the vegetative transition between maize and its progenitor, teosinte. Mol. Plant 10: 1579–1583. https://doi.org/10.1016/j.molp.2017.09.016

Xu, G., X. Wang, C. Huang, D. Xu, D. Li *et al.*, 2017 Complex genetic architecture underlies maize tassel domestication. New Phytol. 214: 852–864. https://doi.org/10.1111/nph.14400

Xu, G., J. Cao, X. Wang, Q. Chen, W. Jin *et al.*, 2019 Evolutionary metabolomics identifies substantial metabolic divergence between maize and its wild ancestor, teosinte. Plant Cell 31: 1990–2009. https://doi.org/10.1105/tpc.19.00111

Yang, C. J., 2018 Dissection of the genetic architecture of domestication traits in maize and its ancestor teosinte. Ph.D. Thesis, The University of Wisconsin–Madison, Madison, WI.

Yang, Q., Z. Li, W. Li, L. Ku, C. Wang *et al.*, 2013 CACTA-like transposable element in *ZmCCT* attenuated photoperiod sensitivity and accelerated the postdomestication spread of maize. Proc. Natl. Acad. Sci. USA 110: 16969–16974. https://doi.org/10.1073/pnas.1310949110

Yu, J., J. B. Holland, M. D. McMullen, and E. S. Buckler, 2008 Genetic design and statistical power of nested association mapping in maize. Genetics 178: 539–551. https://doi.org/10.1534/genetics.107.074245

Zhang, Z., X. Zhang, Z. Lin, J. Wang, M. Xu *et al.*, 2018 The genetic architecture of nodal root number in maize. Plant J. 93: 1032–1044. https://doi.org/10.1111/tpj.13828

Zhao, H., Z. Sun, J. Wang, H. Huang, J. P. Kocher *et al.*, 2014 CrossMap: a versatile tool for coordinate conversion between genome assemblies. Bioinformatics 30: 1006–1007. https://doi.org/10.1093/bioinformatics/btt730

Zhao, Q., A. L. Weber, M. D. McMullen, K. Guill, and J. Doebley, 2011 MADS-box genes of maize: frequent targets of selection during domestication. Genet. Res. (Camb) 93: 65–75. https://doi.org/10.1017/S0016672310000509

Communicating editor: T. Juenger